Magnetic Order in Li-Mn Spinels

C. B. Azzoni, M. C. Mozzati, A. Paleari[a], V. Massarotti[b], D. Capsoni[b] and M. Bini[b]

INFM Department of Physics “A. Volta” of the University, Via Bassi 6, I-27100 Pavia (Italy)
[a] INFM Department of Materials Science of the University, Via Cozzi 53, I-20126 Milan (Italy)
[b] Department of Physical Chemistry of the University and CSTE-CNR, Viale Taramelli 16, I-27100 Pavia (Italy)

Z. Naturforsch. **53a**, 693–698 (1998); received April 25, 1998

Magnetic measurements were carried out on different samples of Lithium-Manganese spinel $LiMn_2O_4$, great care having been taken to avoid the presence of spurious magnetic phases, such as Mn_3O_4. Susceptibility data, showing deviations from paramagnetic behaviour at about 40 K, were analyzed in terms of local magnetic interactions, taking into account the structural and transport properties of these compounds. The magnetic response of pure and stoichiometric samples suggests that the onset of a long-range magnetic ordering is hindered by the topological frustration of the antiferromagnetic octahedral sublattice of the spinel.

Key words: Magnetic Susceptibility; Electron Paramagnetic Resonance; Lithium Manganese Oxides; Lithium Manganese Spinel.

1. Introduction

Lithium manganese spinel based compounds have recently received growing interest as to their application in electrochemistry and catalysis and in lithium ion selective detectors. They are also interesting for the coexistence of Mn^{4+} and Mn^{3+} valence states [1, 2], the latter being a potential Jahn-Teller (JT) ion which may drive structural distortions by cooperative effects [3, 4]. The occurrence of magnetic ordering in these compounds is strictly related to the effective localization of the electrons introduced by Li substitution; so the study of the magnetic features may be useful for the understanding of the transport features of these compounds.

As regards the magnetic susceptibility χ of the stoichiometric $LiMn_2O_4$ spinel, different behaviours are reported [1, 5–9], showing a sample dependent χ-increase at low temperature. The spread of these results is probably related in part to differences in the preparation methods, i.e. difficulty in obtaining pure and really stoichiometric compounds. However, concerning the magnetic properties of the $LiMn_2O_4$ spinel, some common features may be remarked from the observed high temperature paramagnetic behaviour. The negative Weiss temperature θ suggests a prevalent antiferromagnetic character of the local magnetic interactions. Moreover, the calculated magnetic moment per Mn ion [1, 6] is consistent with the coexistence of Mn^{4+} ions ($S=3/2$) with Mn^{3+} ions in the high spin configuration ($S=2$), with the fourth electron in a e_g orbital. This electron localization is supported by charge transport measurements [1], since the rather low conductivity σ ($10^{-4}\ \Omega^{-1}\ cm^{-1}$ at 300 K) and the weak thermal dependence of the thermopower suggest the presence of an electron hopping mechanism with an activation energy of 0.4 eV. Moreover, independent evidence of electron localization in e_g orbitals comes from structural data. In fact, nearly stoichiometric $Li(Li_yMn_{2-y})O_4$ compounds, from Li enrichment of $LiMn_2O_4$ limited in the range $0<y<0.04$, show structural changes with lowering the transition temperature below 280 K [3, 4]. These changes were ascribed to the onset of a cooperative JT transition arising from tetragonal elongation of the coordination octahedra around the Mn^{3+} ions.

This work aims at investigating the magnetic interactions in Lithium-Manganese spinels, by means of susceptibility, magnetization and EPR measurements, in strict connection with structural determinations.

2. Sample Preparation and Structural Details

Several samples were synthesized by a solid state reaction from starting mixtures MnO-Li_2CO_3 with 0.333 Lithium cationic fraction. Each mixture was heated 8 hours in air at 1073 K with heating and cooling rates

---

Reprint requests to Prof. C. B. Azzoni; Fax: 0382-507563.

0932-0784 / 98 / 0800-0693 $ 06.00 © – Verlag der Zeitschrift für Naturforschung, D-72027 Tübingen

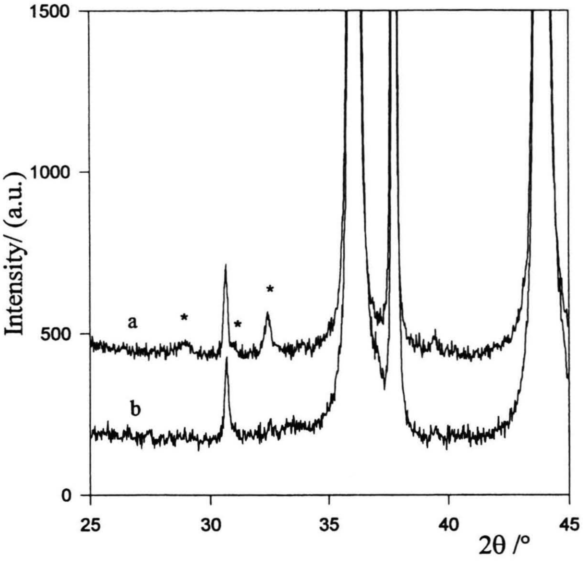

Fig. 1. Comparison of XRD patterns of Lithium-Manganese spinel *a* and *b* in a limited 2θ range: Mn_3O_4 peaks in the *a*-sample are marked by stars.

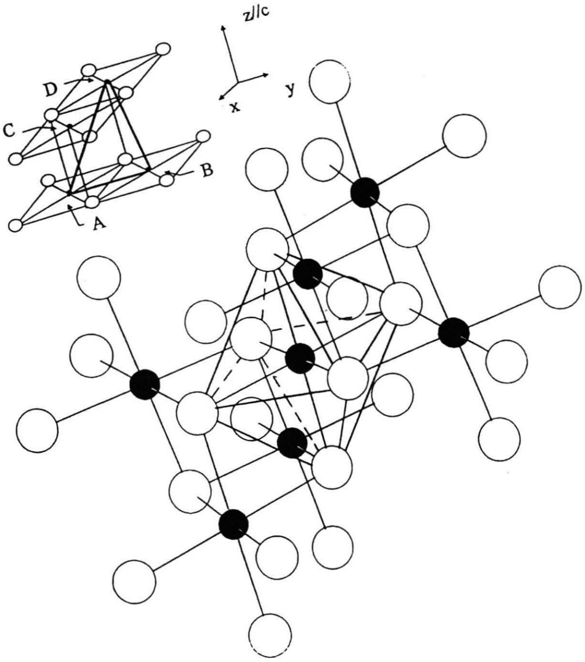

Fig. 2. Coordination oxygen (open circles) octahedra around Mn sites (filled circles) in $LiMn_2O_4$. Six octahedra nearest neighbours to the central one are shown. The inset schematically displays the cluster considered to describe the magnetic interactions and the triangular network of the Mn spinel sublattice.

of 5 K/min: these will be referred to hereafter as *a*-samples.

The characterization by x-ray diffraction of the *a*-samples showed the presence of small amounts of the Mn_3O_4 phase, ferrimagnetic at low temperature [10]. Other procedures were also employed for comparison. Then, one *a*-sample was furtherly treated with particular care, being reheated several times at 1073 K and ground, to assure the complete transformation of the impurity phase, so that its magnetic properties were not affected by the presence of Mn_3O_4 (*b*-sample). Indeed the characterization by x-ray diffraction of the *b*-sample showed the presence of the spinel phase alone, as proved by the pattern comparison (Figure 1). Both spinel lines and the most important peaks of the Mn_3O_4 phase (marked by stars) are present in the *a*-sample, but the latter are absent in the *b*-one.

Besides, the JT transition temperature T_{JT} is a sensitive indicator of the spinel stoichiometry. Actually, T_{JT} changes from 280 K at $y=0$ to 200 K at $y=0.039$ [4], (where y is the Lithium stoichiometry deviation) and at the same time the measured enthalpy of the transition gradually decreases. Our samples, with distinct χ and σ anomalies at 280 K, related to the JT transition [1, 5], may be considered stoichiometric. The value of the lattice parameter (for *a*-sample $a=0.8243(1)$ nm; for *b*-sample $a=0.8239(1)$ nm) is also pertinent to the stoichiometric sample as expected from the comparison with literature values of 0.8246 nm [11].

In order to discuss the physical properties of these compounds, it is important to describe the peculiar Mn sites and the pertinent Mn-O-Mn array. $LiMn_2O_4$ is cubic, spinel type (Fd3m) with atomic positions deduced from [11]. More details about the structure can be given by referring to the coordination octahedra of oxygen ions around the Mn site, as shown in Figure 2. The average Mn-O distance is 0.1983 nm. Six neighboring octahedra are centered on other Mn ions and share the edges with the central one. The Mn-O-Mn angles are about 95° while the O-Mn-O angles are about 85°.

3. Experimental Procedure

Static magnetic susceptibility and magnetization measurements were carried out from 300 K down to 4 K, in magnetic fields ranging between 50 and 4500 G, by using a Faraday balance susceptometer with a continuous-flow cryogenic apparatus. The final accuracy of the mass susceptibility (χ_m) data results in an error of a few %. The magnetic field dependence was analyzed by changing the field intensity at fixed temperatures.

EPR measurements were carried out by using a Bruker spectrometer at 9.12 GHz between 120 and 473 K.

Diffraction data were obtained by a Philips PW1710 powder diffractometer equipped with a Philips PW1050 vertical goniometer. Use was made of the CuKα radiation (Kα_1=1.54056 Å; Kα_2=1.5443 Å) by means of a graphite monochromator. Patterns were collected in the angular range $15° < 2\theta < 130°$ in the step scan mode (step width 0.025°; counting time 10 s). Further details and computational procedure have been given in [1, 2].

4. Results

In Fig. 3 the $\chi_m(T)$ and $\chi_m^{-1}(T)$ curves of the *b*-sample are reported down to 4 K. The change in the slope of $1/\chi_m$ at about 40 K might suggest the onset of a magnetic ordering. The paramagnetic region is not characterized by a well defined Weiss temperature θ because for $T > 280$ K a pronounced deviation from linearity is observable. However, a negative temperature intercept $\theta \cong -320$ K may be argued. This value is confirmed in [8], where the $\chi_m^{-1}(T)$ curve is reported up to 800 K. For the same sample, data of the mass magnetization M vs. applied field at different temperatures are reported in Figure 4. M follows linear behaviours strictly proportional to the field intensity, also below 40 K, as in non magnetically ordered compounds. The extrapolated zero field $M(0)$ values are reported in Fig. 5, as functions of the temperature for the *b*- and *a*-sample. Only the *a*-sample shows a weak net resultant magnetic moment, due to the presence of few % of Mn_3O_4 phase (≈1.5%) (see the inset of Fig. 5), while the *b*-sample shows a negligible $M(0)$ value. This behaviour of $M(0)$ confirms the lack of Mn_3O_4

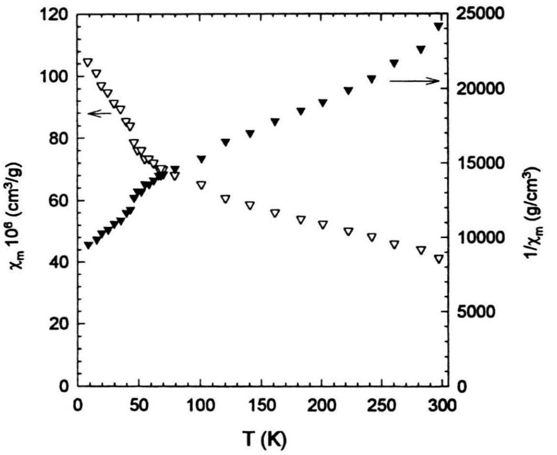

Fig. 3. Temperature dependence of χ_m (open marks) and χ_m^{-1} (filled marks) of the *b*-sample.

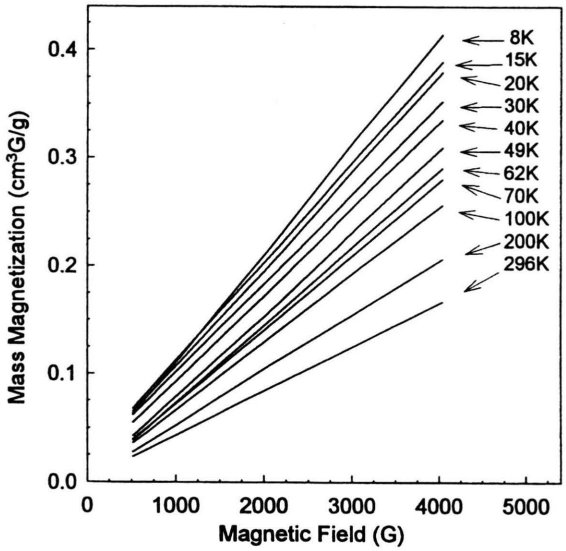

Fig. 4. Mass magnetization curves at different temperatures of the *b*-sample.

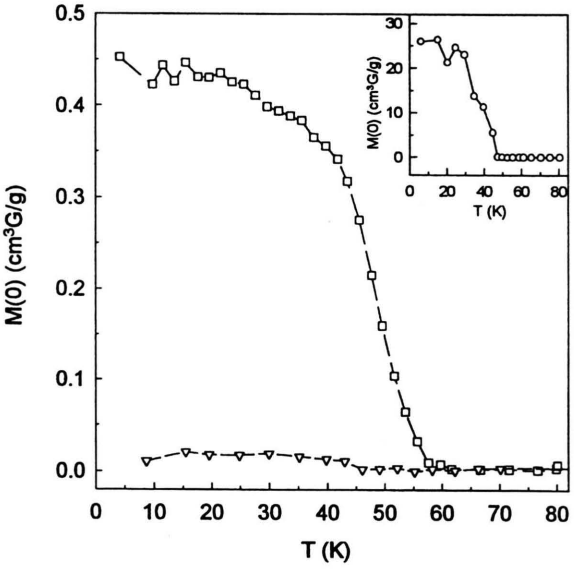

Fig. 5. Mass magnetization curves vs. Temperature of the *b*-sample (triangles), of an *a*-sample (squares) and of Mn_3O_4 (inset).

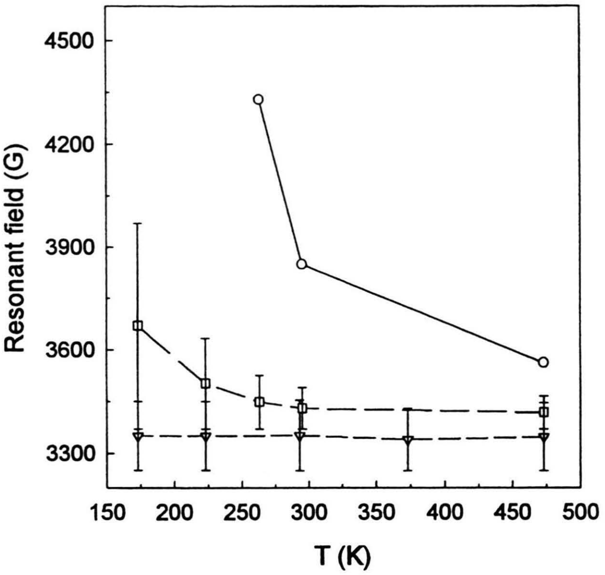

Fig. 6. Resonant field vs. Temperature of the EPR signal for the *b*-sample (triangles), an *a*-sample (squares) and Mn_3O_4 (circles).

phase in the reheated spinel. This assertion is also supported by Fig. 6, reporting the different behaviour of the resonant field (RF) of EPR spectra for spinel samples and Mn_3O_4: only the *b*-sample shows a RF which does not depend on the temperature while the RF behaviour of the *a*-sample is similar to that observed in Mn_3O_4, although less pronounced.

5. Discussion

At a first glance, the $1/\chi_m$ curve in the spinel (Fig. 3) suggests an antiferromagnetic-like behaviour below 40 K, as also reported in [8]. This is also consistent with the negative θ of the paramagnetic phase, i.e. with a prevalent AF character of the local magnetic interactions. Nevertheless, we cannot observe a clear-cut magnetic transition but only a deviation from the paramagnetic regime, suggesting that the onset of a true magnetic ordered phase is hindered.

Consideration of structural and transport features of these materials may clarify the origin of this behaviour. The electronic conduction is characterized by the hopping of electrons through Mn^{4+} ions, and this is consistent with the value of the conductivity at high temperature (a few Ω^{-1} cm^{-1} at about 1000 K) [1]. Nevertheless, the hopping conductivity at room temperature is very low, and the electrons are to be considered effectively localized in Mn^{4+} to form Mn^{3+} sites. This localization is evidenced by the JT distortion, which pertains to the d^4 configuration of the Mn^{3+} ions. The discussion of the magnetic properties will now be done, starting from the analysis of the possible interaction pictures in the local environments of the Mn sites, in order to permit a comparison with the experimental data.

We remark that the cubic to tetragonal transition at 280 K of the $Mn^{3+}O_6$ octahedra splits the energy levels of the e_g orbitals. By performing crystal field calculations on the octahedral coordination, according to the distortion $c/a = 1.011$ [3], we obtained an energy splitting of 0.08 eV between the d_{3z2-r2} and the d_{x2-y2} states, with the former at lower energy. In the case of Mn^{3+} in high spin configuration, the d_{3z2-r2} state is half-filled while the d_{x2-y2} one is empty. These orbitals should give the main contribution to 90° superexchange interactions via oxygen orbitals. Even though in the stoichiometric spinel each Mn ion has six next neighbours, at a mean distance of 0.2916 nm, it is convenient to consider the possible interactions within the cluster, or magnetic and structural unit, reported in the inset of Fig. 2, which generates the spinel lattice by translation.

The following cases regard superexchange interactions mediated by a single oxygen orbital: between A and B ions (see Fig. 2), two ferromagnetic (F) interactions with ($\sigma\pi$) character from the overlap between d_{x2-y2} and d_{xy} and two antiferromagnetic (AF) ($\pi\pi$) interactions from the overlap of d_{yz} and d_{xz}. Between A and C, D ions, two F interactions occur with ($\sigma\pi$) character between d_{x2-y2} and d_{xz} (or d_{yz}) and two AF ($\pi\pi$) interactions between d_{xy} and d_{xz} (or d_{yz}) (Fig. 7 (I, II)). This process should not be likely, owing to the high energy of the excited levels due to Coulomb interaction. Moreover, all these superexchange contributions should be rather small involving weak π overlap between p and d orbitals.

Superexchange interactions via two orthogonal oxygen orbitals are also possible: one F ($\sigma\sigma$) between A and B ions, and another F ($\sigma\sigma$) between A and C, D ions arising from the overlap of e_g orbitals with p oxygen orbitals taking into account the Hund rule for the spins of the two half-filled orbitals of the oxygen (Fig. 7 (III)). The full σ character of these interactions suggests that these should prevail over the others, also because they do not call for orbitals already involved into direct interactions.

In fact, since the coordination octahedra share a common edge, direct magnetic interactions take place between Mn ions through half-filled t_{2g} orbitals [12]. These interactions are AF and the more intense the smaller the

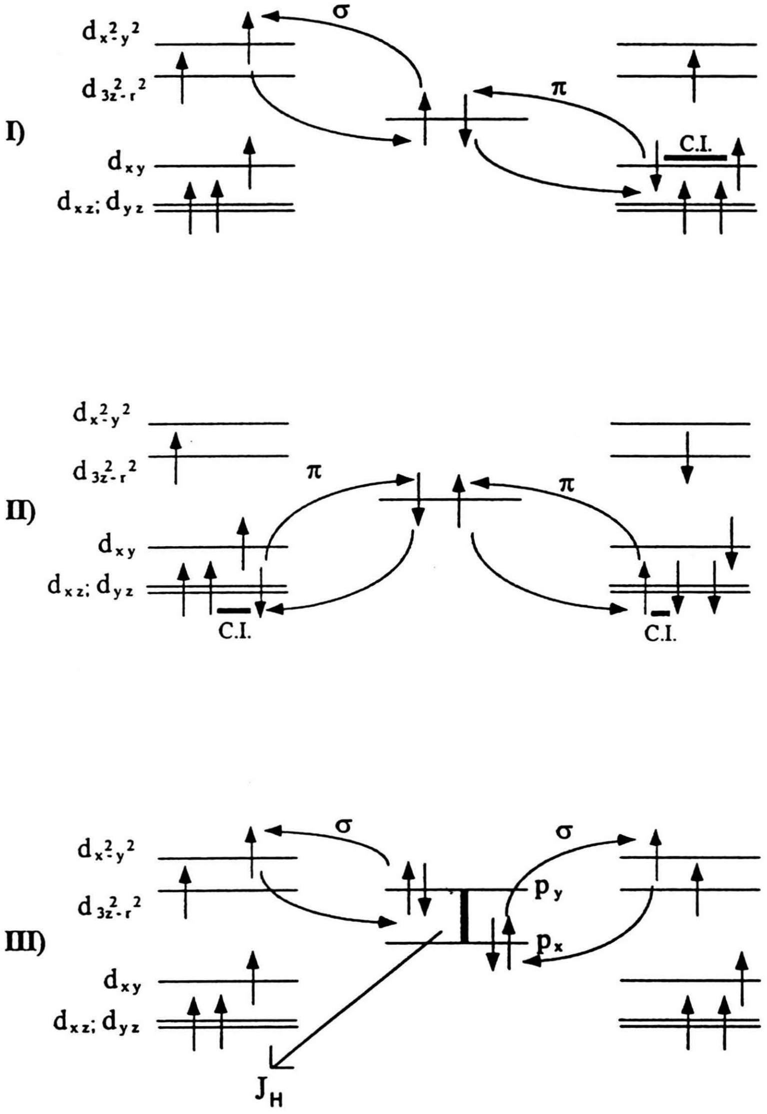

Fig. 7. Magnetic interaction mechanisms in Mn^{3+}-O-Mn^{3+} complexes via one oxygen p-orbital (I and II) and two oxygen p-orbitals (III): (I) ferromagnetic interaction $d_{x2-y2}-p-d_{xy}$; (II) antiferromagnetic interaction $d_{xy}-p-d_{zx}$; (III) ferromagnetic interaction $d_{x2-y2}-p_y:p_x-d_{x2-y2}$. The same mechanisms hold in the cases of $Mn^{3+}-O-Mn^{4+}$ and $Mn^{4+}-O-Mn^{4+}$ interactions, provided that the d_{3z2-r2} orbital of one or both cations, respectively, is empty. The Hund's rule interaction is indicated by J_H, and the Coulomb interaction by C.I.

distance between the cations. A direct AF interaction will be active between d^3-d^3 or d^4-d^4 and d^3-d^4 ion couples through the overlap of d_{xy}, d_{xz} and d_{yz} orbitals.

In summary, the A–C, D interaction results from two direct AF and a superexchange F one, while the resulting A–B interaction arises from a direct AF interaction and a superexchange one comprising F contributions. Both could be in principle either F or AF, but experimental data and transport and structural features of these compounds (similarly to other insulator oxides with half-filled t_{2g} orbitals [12, 13]) suggest that the direct interactions play the relevant role in determining the magnetic properties, and the resulting local interactions should be AF.

Consideration of the local geometry in the spinel lattice (see Fig. 2) shows that magnetic ions lie in the sites of a triangular network of the transition cation sublattice. No magnetic long-range ordering of spins is possible, because of the frustration of the AF interaction between some ion pairs. This is a typical situation occurring in an octahedral AF sublattice giving rise to a spin-glass type behaviour, according to [9]. By contrast, more evident deviations or magnetic transitions observed in the same range of temperature in other spinel samples (as in our *a*-samples) are to be attributed to spurious magnetic phases, as ferrimagnetic Mn_3O_4.

6. Conclusion

Susceptibility and magnetization measurements, compared with data from conductivity [1], thermal analysis [3, 4], and x-ray powder diffraction [2] measurements, allowed us to put forward a correlation among electron localization, onset of cooperative JT effect and magnetic features below 40 K in the $LiMn_2O_4$ spinel.

The magnetic response of pure and stoichiometric samples was detailed by considering the possible local magnetic interactions consistent with the structure. This analysis, together with geometrical arguments on the magnetic sublattice, suggests that the onset of a long-range magnetic ordering is hindered by the topological frustration of the antiferromagnetic octahedral sublattice of the spinel.

Acknowledgements

This work has been partially supported by Consorzio per i Sistemi a Grande Interfase (CSGI) and by Progetto Finalizzato MSTA II-Accumulo di Energia.

[1] V. Massarotti, D. Capsoni, M. Bini, G. Chiodelli, C. B. Azzoni, M. C. Mozzati, and A. Paleari, J. Solid State Chem. **131,** 94 (1997).
[2] V. Massarotti, D. Capsoni, M. Bini, C. B. Azzoni, and A. Paleari, J. Solid State Chem. **128,** 80 (1997).
[3] A. Yamada and M. Tanaka, Mat. Res. Bull. **30,** 715 (1995).
[4] A. Yamada, J. Solid State Chem. **122,** 160 (1996).
[5] J. Sugiyama, T. Tamura, and H. Yamauchi, J. Phys.: Condensed Matter **7,** 9755 (1995).
[6] C. Masquelier, M. Tabuchi, K. Ado, R. Kanno, Y. Kobayashi, Y. Maki, O. Nakamura, and J. B. Goodenough, J. Solid State Chem. **123,** 255 (1996).
[7] N. Kumagai, T. Fujiwara, K. Tanno, and T. Horiba, J. Electrochem. Soc. **143,** 1007 (1996).
[8] J. Sugiyama, T. Hioki, S. Noda, and M. Kontani, J. Phys. Soc. Japan **66-1,** 1187 (1997).
[9] P. Endres, B. Fuchs, S. Kemmler-Sack, K. Brandt, G. Faust-Becker, and H.-W. Praas, Solid State Ionics **89,** 221 (1996).
[10] B. Boucher, R. Buhl, and M. Perrin, J. Phys. Chem. Solids **32,** 2429 (1971).
[11] D. G. Wickham and W. J. Croft, J. Phys. Chem. Solids **7,** 351 (1958).
[12] J. B. Goodenough, Phys. Rev. **117,** 1442 (1960).
[13] V. Massarotti, D. Capsoni, M. Bini, C. B. Azzoni, M. C. Mozzati, and A. Paleari, Z. Naturforsch. **53 a,** 150 (1998).